Precision SAR Processing Using Chirp Scaling

R. Keith Raney, *Fellow, IEEE,* H. Runge, Richard Bamler, Ian G. Cumming, and Frank H. Wong

***Abstract*—A space-variant interpolation is required to compensate for the migration of signal energy through range resolution cells when processing synthetic aperture radar (SAR) data, using either the classical range/Doppler (R/D) algorithm or related frequency domain techniques. In general, interpolation requires significant computation time, and leads to loss of image quality, especially in the complex image. The new *chirp scaling* algorithm avoids interpolation, yet performs range cell migration correction accurately. The algorithm requires only complex multiplies and Fourier transforms to implement, is inherently phase preserving, and is suitable for wide-swath, large-beamwidth, and large-squint applications. This paper describes the chirp scaling algorithm, summarizes simulation results, presents imagery processed with the algorithm, and reviews quantitative measures of its performance. Based on quantitative comparison, the chirp scaling algorithm provides image quality equal to or better than the precision range/Doppler processor. Over the range of parameters tested, image quality results approach the theoretical limit, as defined by the system bandwidth.**

I. Introduction

RECENT advances in synthetic aperture radar (SAR) image analysis impose increased requirements on the precision of image products, particularly the fidelity of the complex image. Pertinent applications include SAR interferometry, quadrature polarimetry, complex speckle reduction filter techniques, and complex signal analysis for system calibration.

The performance and precision of SAR processing techniques are summarized in [1]. The most popular SAR processing algorithm is the range/Doppler (R/D) technique, and variations of it. This method is efficient, and in principle, solves the problems of azimuth focusing and range cell migration correction (RCMC). The main disadvantages of R/D processors are that: 1) the secondary range compression cannot easily incorporate azimuth frequency dependence, and 2) RCMC requires an interpolator. To achieve accurate results, the kernel of the interpolator must have range-varying coefficients, and should span many samples. In practice, this leads to a less than ideal accuracy/efficiency tradeoff. Most processors use 4–8 point kernels, which favors the efficiency side of the tradeoff: precision SAR processing loses out in the bargain.

Several researchers [6], [17] have examined SAR processing algorithms based on the seismic wave equation formulations [22], [5]. Wavenumber domain methods have the advantage of dealing directly with the natural polar coordinate system arising from wave propagation, and achieve most signal processing operations in the two-dimensional frequency domain with a relatively simple phase multiply. The dominant disadvantage of wavenumber domain approaches is that an interpolator is needed to match the range-dependent RCMC parameter variations, either for the Stolt change of variables in the two-dimensional frequency domain [5] or for the residual RCMC in the range/Doppler domain [17].

The contribution of the present work is a SAR processing algorithm that retains reasonable efficiency, while at the same time it eliminates approximations arising from the truncated interpolation kernel normally used to achieve RCMC. The method is the *chirp scaling algorithm* [20], also known as the differential range deramp or DRD algorithm [8]. The particular approach used in our chirp scaling algorithm produces excellent radiometric and geometric results, and is inherently phase preserving.

The analytical foundation for the treatment is presented in Section II. The chirp scaling algorithm is described in Section III. Critical analysis of image quality based on simulated signals is outlined in Section IV, and image quality based on actual SAR data is described in Section V. Following comments on implementation issues in Section VI, conclusions appear in Section VII. Three Appendixes are included that provide more detailed consideration of the performance of the chirp scaling approach.

II. Problem Statement

The data available to a SAR processor are an ensemble of two-dimensional dispersed signals. Each signal consists of the record of reflections from an individual scatterer in the illuminated scene. Scene coordinates, with respect to the radar motion vector, are *azimuth* (scatterer location along the vector) and *range* (scatterer orthogonal distance from the vector). Signal coordinates are similar, but include a subtle yet essential difference: range in the signal domain is the instantaneous distance from the antenna to each scatterer. In general, range is not orthogonal to azimuth in signal space.

The task of the processor is to implement a filter, matched in both the range and azimuth directions, to fo-

Manuscript received March 11, 1993; revised January 10, 1994 and March 1, 1994.

R. K. Raney is with The Johns Hopkins University, Applied Physics Laboratory, Laurel, MD, USA, 20723-6099. The work of this paper was performed while he was at the Canada Centre for Remote Sensing (CCRS), Ottawa, Ont., Canada, K1A 0Y7.

H. Runge and R. Bamler are with the German Aerospace Research Establishment (DLR), Oberpfaffenhofen, Germany.

I. G. Cumming is with the Department of Electrical Engineering, University of British Columbia, Vancouver, B.C., Canada V6T 1Z4.

F. H. Wong is with MacDonald Dettwiler, Richmond, B.C., Canada V6V 2J3.

IEEE Log Number 9402666.

cus the signal data. The design problem is challenging because: 1) the range and azimuth coordinates are coupled in the signal impulse response (range curvature or range cell migration), and 2) the amount of range cell migration depends on range.

A. Signal Impulse Response

In signal space, after demodulation, the response from a point scatterer (Fig. 1) located at range r and at azimuth time $t = 0$ for azimuth antenna weighting $a(\cdot)$ and transmitted signal envelope $s_0(\cdot)$ is

$$pp(\tau, t; r) = a(t, r)s_0\left(\tau - \frac{2R(t; r)}{c}\right) \cdot \exp\left\{-j\frac{4\pi}{\lambda}R(t; r)\right\} \quad (1)$$

where t is time along the radar flight path, τ is delay time in the (slant) range direction, c is the speed of light, and λ is the radar wavelength. The purpose of the $pp(\cdot)$ notation is explained below. The time-varying distance from the radar to the scatterer is given by the range delay term

$$R(t; r) = \sqrt{r^2 + V^2(r)t^2} \quad (2)$$

where $V(r)$ is the relative velocity proportionality parameter between the scatterer and the radar, scaled to account for the curved orbit, and earth curvature and rotation. For narrow beam systems operating relatively close to the observed scene, such as for most aircraft radars, the relative velocity is virtually equivalent to sensor speed and not dependent on range, but for a more generalized geometry, such as the satellite SAR case, the velocity parameter $V(r)$ is a function of range [14], which needs to be included for precision processing. Range delay in (2) is with respect to the scatterer's range r of closest approach, assumed to be observed by the radar at zero azimuth time t.

The range/azimuth dependence of the range delay term impacts both the phase and the envelope location of the signal impulse response (1). SAR focusing in azimuth is done by matching the azimuth phase modulation imposed on all signals through the systematic range changes from (2). If the change in range of the focused pulse is larger than the range sample spacing, then the signals follow loci that cross range pixel boundaries in signal space. This phenomenon is known as range cell migration. In order for the processor to compress the azimuth dimension of the signal, either the filter must follow the curve of the signal locus (which requires a time-domain interpolation) or the range delay locus must be straightened (which is the task of the RCMC procedure). Once RCMC has been done, then the azimuth filter requires only a simple one-dimensional operation.

B. Two-Dimensional Frequency Domain

The range cell migration from one scatterer, as shown in Fig. 1, could be straightened by warping the signal space or, equivalently, by changing the range scale of the

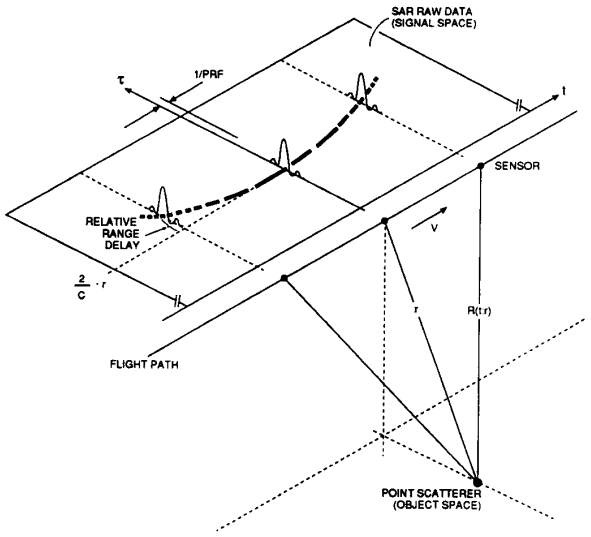

Fig. 1. Transformation of signal history from object space into signal space.

domain as a function of azimuth time t to counteract the delay term of (2). However, if there are several signals from different azimuth locations simultaneously present, as must be true in a practical case, then their loci overlap. Hence, it is impossible to correct all range cell migrations by a simple range-proportional scaling in the signal domain.

In principle, application of a two-dimensional linear time-domain filter over the received signals simultaneously could perform compression and correct range cell migration [23], although a new filter would be required for each range cell. Implementation in the time domain requires many more operations, resulting in a comparatively slow processor. We confine our discussion to transform domain techniques.

The two-dimensional Fourier transform of the signal impulse response has the form

$$PP(f_\tau, f; r) \sim A(\cdot)S_0(\cdot)\exp\{j\varphi(f_\tau, f; r)\} \quad (3)$$

where the capital letters PP indicate the Fourier transform of the range and azimuth functions pp, respectively, and (f_τ, f) are the frequency variables corresponding to range time and azimuth time (τ, t), respectively. The functions $A(\cdot)$ and $S_0(\cdot)$ are the transforms of the antenna weighting and the pulse envelope. Using a Taylor series expansion on range frequency, the phase term of the generic two-dimensional signal transform has leading terms

$$\varphi(f_\tau, f; r) = \varphi_0(f; r) + \varphi_1(f; r)f_\tau + \varphi_2(f; r)f_\tau^2 + \cdots. \quad (4)$$

Each phase term in (4) is significant in the development of our algorithm. Higher order terms in general are not significant in most radar specific applications.

The first term of (4), constant in range frequency f_τ, carries the phase information required to focus the data in the azimuth direction. The second phase term of (4), linear in f_τ, carries both the correct range position of the scatterer (desired) and the range cell migration (undesired), which is to be compensated. The third phase term, quadratic in f_τ, contains a dispersion of the range pulse that becomes larger with increasing squint angles. Conventional means for its correction include a change of variables [22] in active seismic work, and adjustment of the range FM rate [10] used in SAR, in which case it is known as secondary range compression (SRC). Range/Doppler algorithms are not able to adjust the SRC term φ_2 with respect to Doppler f or range r without increasing the computational load. The desirability to take the Doppler dependence of the SRC term into account has been noted in the literature [7], [24], [21].

The range cell migration term is dependent on range. Note that range is not available as an independent parameter in the two-dimensional frequency domain. When there are several signals from different range locations simultaneously present, as is generally the case, then their transforms overlap. A fixed value of the range parameter corrects range cell migration for one specific range position, but signals from all other ranges have only an approximate correction applied. Thus, *it is not possible to correct fully for range cell migrations using linear filters in the two-dimensional transform domain* when no other RCMC stages are used.

C. Range/Doppler Domain

In the range/Doppler domain, which is the "natural" coordinate system for this class of coherent radars, there is a unique and single-valued (one-to-one) relationship between the geometry of each and every illuminated scatterer and the signal histories $pP(\tau, f)$ available. [The utility of the lower case/upper case naming convention for two-dimensional functions is now clear, here denoting time domain for the first variable (τ), and frequency domain for the second variable (f).] In the range/Dopper domain, multivalued (many-to-one) superposition of different range cell migrations is eliminated in azimuth, and access to the range parametric variation is retained. Conventional R/D SAR processors rely on this single-valued property to realize RCMC.

An analytic expression for the range/Doppler form of the signal impulse response cannot be derived for arbitrary pulse modulation. The expression is known, however, for the case in which there is a large time–bandwidth phase modulation on the transmitted signal. We assume that the radar uses chirp modulation, e.g., linear FM (frequency modulation), of rate K. The baseband signal impulse response takes the more specific form

$$pp(\tau, t; r) = a(t)\, s_0\left(\tau - \frac{2}{c} R(t; r)\right) \exp\left\{-j\pi K\left(\tau - \frac{2}{c} R(t; r)\right)^2\right\} \exp\left\{-j\frac{4\pi}{\lambda} R(t; r)\right\}. \tag{5}$$

By application of the principle of stationary phase (e.g., [4]), it may be shown (Wong, unpublished notes and [15]), within an arbitrary complex constant $\mathbb{C}$, that the corresponding range/Doppler transform may be written

$$\begin{aligned} pP(\tau, f; r) = {} & \mathbb{C}a\left(-\frac{rf\lambda}{2V^2}\right) s_0\left(\tau - \frac{2}{c} R_f(f; r)\right) \\ & \cdot \exp\left\{-j\pi K_s(f; r)\left(\tau - \frac{2}{c} R_f(f; r)\right)^2\right\} \\ & \cdot \exp\left\{-j\frac{4\pi r}{\lambda}\left[1 - \left(\frac{\lambda f}{2V(r)}\right)^2\right]^{1/2}\right\} \end{aligned} \tag{6}$$

where the parameter $V(r)$, in general, includes a small range dependence due to orbit curvature, combined with Earth curvature and rotation. For the derivation of (6), $V(r)$ is assumed to be constant in the neighborhood of each stationary point (Appendix B).

D. Range Curvature Factor

The range/Doppler expression of (6) introduces two new functions. The time domain range delay (2) carries over into the range/Doppler domain as

$$R_f(f; r) = \frac{r}{\sqrt{1 - \left(\frac{\lambda f}{2V(r)}\right)^2}} \tag{7}$$

which has the functional form

$$R_f(f; r) = r[1 + C_s(f)] \tag{8}$$

where

$$C_s(f) = \frac{1}{\sqrt{1 - \left(\frac{\lambda f}{2V(r)}\right)^2}} - 1 \tag{9}$$

is the *curvature factor*, which describes the Doppler frequency-dependent part of the signal trajectory. The curvature factor $C_s(f)$ is a strong function of f, but only mildly dependent on range r. (The body of this paper treats this factor as locally constant with respect to range. Extension of the work to range variation is covered in Appendix B.)

The term $R_f(\cdot)$ (7) describes range migration in the range/Doppler domain through the position shift in the range signal envelope $s_0(\cdot)$ of (6). The delay is a function of both Doppler f and scatterer range r, and is single valued at every point. Thus, there is a family of range/Doppler loci that describe the distribution of range cell migrations over the entire range/Doppler plane, as suggested in Fig. 2.

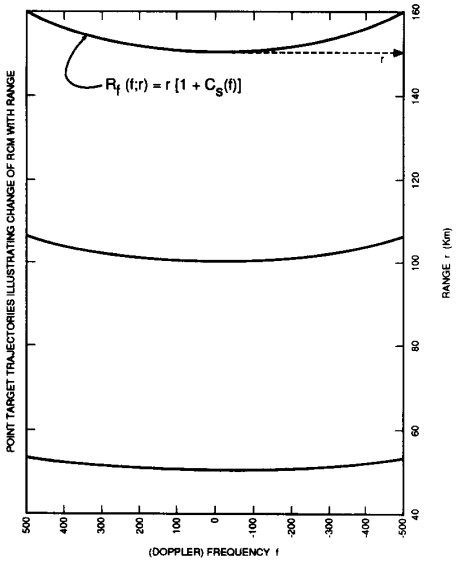

Fig. 2. Range cell migration in the range/Doppler domain.

E. Range Phase Distortion

The second new function of (6) is the effective FM chirp rate in range,

$$K_s(f;r) = \frac{K}{1 + Kr\frac{2\lambda}{c^2}\frac{\left(\frac{\lambda f}{2V(r)}\right)^2}{\left[1 - \left(\frac{\lambda f}{2V(r)}\right)^2\right]^{3/2}}} \tag{10}$$

which has the functional form

$$\frac{1}{K_s(f;r)} = \frac{1}{K} + r\alpha(f;r) \tag{11}$$

where

$$\alpha(f;r) = \frac{2\lambda}{c^2}\frac{\left(\frac{\lambda f}{2V(r)}\right)^2}{\left[1 - \left(\frac{\lambda f}{2V(r)}\right)^2\right]^{3/2}} \tag{12}$$

is the *range distortion factor*. This factor, which leads to range defocus if not compensated, has a strong dependence on Doppler f, but only a weak dependence on range. The range distortion, $r\alpha(f;r)$ in (11), when matched in the processor, achieves so-called *secondary range compression* (SRC) [10], [24], [1]. Note that the range distortion is not a function of the FM rate K: rather, it is a function of the geometry. Range distortion is a direct consequence only of the lack of orthogonality between "range" and "azimuth" for signal components away from zero Doppler, and applies to any form of range modulation, not just to linear FM.

III. Chirp Scaling Algorithm

The chirp scaling algorithm is designed around *curvature equalization*, so that by the time the signal is transformed to the two-dimensional frequency domain, all of the range cell migration trajectories have been adjusted to have congruent loci, equivalent to the trajectory of a scatterer at the selected reference range r_{ref}. As all of the resulting range migration trajectories are single valued in the two-dimensional frequency domain, then RCMC may be completed by a phase multiplication that is known and single valued at each and every point.

Curvature equalization is done simply, yet accurately, by application of a phase multiplication in the range signal/Doppler domain. If the radar uses a large time–bandwidth signal modulation having a dominant linear FM characteristic, then there exists a unique solution. The required function, which depends on Doppler frequency, has quadratic phase modulation in range, whose FM rate is very small compared to the FM rate of the range pulse modulation. The equalizing phase function causes a range/Doppler-dependent change in range scale over signal space. Secondary range compression may be implemented by using a range compression filter whose rate is (mildly) Doppler frequency dependent.

The chirp scaling algorithm uses operations in both the range/Doppler domain and the two-dimensional frequency domain. Rather than completing range compression first, the chirp scaling algorithm starts and finishes with azimuth transforms; range operations are embedded in the middle. The logical flow diagram of the chirp scaling algorithm is shown in Fig. 3. Note that only multiplications and Fourier transforms are required. There are no interpolations needed for complete RCMC. As shown in the figure, the output file consists of a single look complex (SLC) image. In the following, we discuss the key steps in the algorithm: issues such as detection and multilooking not specific to this algorithm are not featured in the development. The canonic form of the basic chirp scaling operation as it is known in classical filter analysis is outlined in Appendix A.

A. Azimuth FFT

Having available a block of raw data, the first step is an FFT in the azimuth direction, which carries the signal data to the range signal/Doppler domain. At this stage, it is helpful to distinguish between the "range (image)/Doppler" domain and the "range *signal*/Doppler" domain. Since the signal is characterized by a large time–bandwidth product, there is a degree of freedom available in the signal domain that is not available in the compressed range (image) dimension. The algorithm exploits the linear FM signal structure that exists only prior to range compression.

The azimuth FFT imposes two extra corner turns on the processing budget of this algorithm when compared to the conventional R/D approach. However, with the large computer main memories available today, it is possible to hold the data for a whole processing block and access them easily in two dimensions.

Following the azimuth FFT, the signal is described by (6) above, which serves as the starting point for the present development.

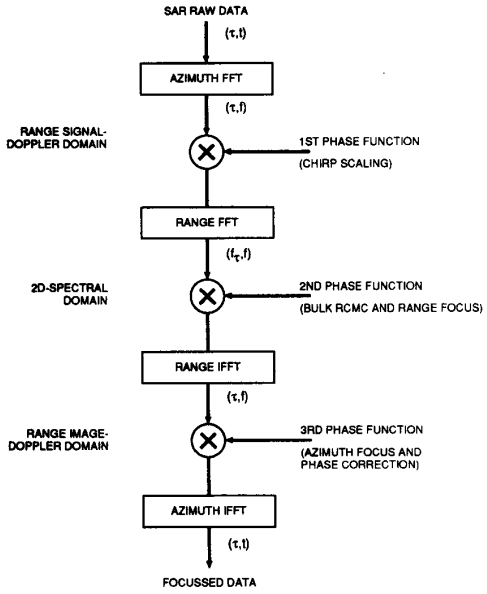

Fig. 3. Flow diagram of the chirp scaling algorithm.

B. Chirp Scaling Phase Multiply

While in the range signal/Doppler domain, the data array is multiplied by a function whose phase is chosen so that the range migration phase term of each and every scatterer is equalized to that of the *reference range*. The spatial loci of the resulting range curvatures are illustrated in Fig. 4, shown as they would appear after range focusing. In principle, the choice of the reference locus is not critical, and even may be outside the swath being imaged. The time locus of the reference range in the range signal/Doppler domain is

$$\tau_{\text{ref}}(f) = \frac{2}{c} r_{\text{ref}}[1 + C_s(f; r)]. \tag{13}$$

If the problem is posed with an unknown FM rate for the quadratic phase multiply, then elimination of the range-varying curvature terms leads to a unique solution [16]. The required chirp scaling multiplier is [20]

$$\Phi_1(\tau, f; r_{\text{ref}}) = \exp\{-j\pi K_s(f; r_{\text{ref}}) C_s(f)[\tau - \tau_{\text{ref}}(f)]^2\}. \tag{14}$$

The *chirp scaling* parameter $C_s(f)$ is the curvature factor of (9). The effective FM rate $K_s(f; r_{\text{ref}})$ includes Doppler variation for SRC, although the range parameter must be set to a constant r_{ref}, which is an approximation of minor consequence (Appendix C). All parameters of the first phase multiplier function $\Phi_1(\cdot)$ are single valued and known over the range signal/Doppler domain.

Multiplication by $\Phi_1(\cdot)$ causes a very small range and Doppler-dependent deformation of each range chirp phase structure so that the phase centers of all signals follow the same reference curvature trajectory:

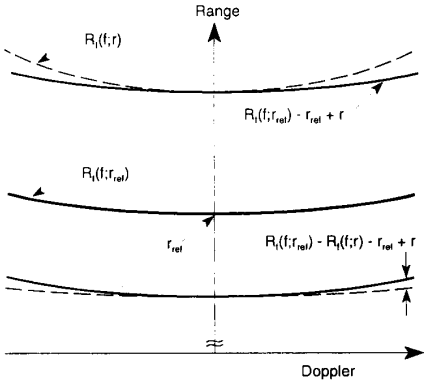

Fig. 4. Equalized range curvatures resulting from the chirp scaling algorithm.

$$\tau(f) = \frac{2}{c}[r + r_{\text{ref}} C_s(f)]. \tag{15}$$

Note, however, that the positions of the chirp envelopes s_0 have not been shifted.

The chirp scaling function of (14) is exactly linear FM (i.e., a quadratic function of τ) only if: 1) the radar pulse is linear FM, and 2) the azimuth FM rate parameter $V(r)$ is constant with range. In practice, $V(r)$ is range dependent, and the range chirp may not be perfectly linear. These situations may be handled directly in the algorithm by inclusion of a matching nonlinear component in the chirp scaling phase multiply (Appendix B).

C. Range FFT

The effect of the chirp scaling phase multiply is evident after application of the range FFT. The result is the two-dimensional frequency domain expression

$$\begin{aligned} PP(f_\tau, f) = {} & \mathbb{C}a\left(-\frac{r\lambda f}{2V^2(r)}\right) s_0\left(-\frac{f_\tau}{K_s(1 + C_s)}\right) \\ & \cdot \exp\left\{-j\frac{4\pi}{\lambda} r\left[1 - \left(\frac{\lambda f}{2V(r)}\right)^2\right]^{1/2} \right. \\ & \left. - j\Theta_\Delta(f; r)\right\} \\ & \cdot \exp\left\{+j\pi \frac{f_\tau^2}{K_s(f; r_{\text{ref}})[1 + C_s(f)]}\right\} \\ & \cdot \exp\left\{-j\frac{4\pi}{c} f_\tau[r + r_{\text{ref}} C_s(f)]\right\} \end{aligned} \tag{16}$$

where

$$\Theta_\Delta(f; r) = \frac{4\pi}{c^2} K_s(f; r_{\text{ref}})[1 + C_s(f)] C_s(f)(r - r_{\text{ref}})^2. \tag{17}$$

Each phase term of (16) has a direct interpretation. The first phase function is the azimuth modulation, which is

constant with respect to the range (frequency) variable. It includes a parametric dependence on range r (17) which is matched in the range/Doppler phase multiplier Φ_3 as discussed below.

The second phase term of (16), quadratic in range frequency f_τ, is the effective range chirp modulation, whose initial FM rate K has been modified by the range curvature, and modified even more by the Doppler-dependent FM rate of the chirp scaling applied during the previous step. The effective FM rate parameter may be rewritten in the form

$$\frac{1}{K_s(f; r_{\text{ref}})[1 + C_s(f)]} = \frac{1}{K[1 + C_s(f)]} + \frac{\alpha(f; r_{\text{ref}})}{1 + C_s(f)} r_{\text{ref}} \quad (18)$$

which shows that the chirp scaled FM rate (the first term on the right-hand side of the equation) and the geometric phase distortion (the second term) are separable and additive. The chirp scaled FM rate is single valued and known over the two-dimensional frequency domain, and may be exactly compensated (discussed in the following section). The second term in (18) is proportional to target range, and therefore, when several signals are present simultaneously, it is multivalued in the frequency domain. However, range-dependent variations are very small when compared to the magnitude of the FM rate term so that use of a constant r_{ref} in this term is satisfactory. Variations due to the Doppler frequency parameter f may be matched in this domain.

The third phase term of (16), linear in range frequency f_τ, carries the correct range position r of each scatterer as well as its range curvature. Thanks to the previous chirp scaling multiply, however, the relative range curvature is $R_f(f; r_{\text{ref}})$, which is the same value for all ranges; hence, it is single valued over the two-dimensional frequency domain.

D. RCMC, Range Compression, and SRC Multiply

Range cell migration correction (RCMC) and range focus, including secondary range compression (SRC) with its Doppler-dependent variation and compensation for the chirp scaling change in FM rate, may be done with a phase multiplication by a function whose value is known at each point on the two-dimensional space. The phase multiplication is

$$\Phi_2(f_\tau, f; r_{\text{ref}}) = \exp\left\{-j\pi \frac{f_\tau^2}{K_s(f; r_{\text{ref}})[1 + C_s(f)]}\right\} \cdot \exp\left\{+j \frac{4\pi}{c} f_\tau r_{\text{ref}} C_s(f)\right\}. \quad (19)$$

The first factor achieves range focus including SRC. The RCMC is done by the second factor. Since it corrects the dominant range curvature effects in a satellite SAR geometry, it is known as the *bulk RCMC*. (Likewise, bulk azimuth compression could be done at this stage, although for this discussion, we choose to perform all azimuth focusing operations at one time, as described below.) Note that $C_s(f)$ is a function of $V(r)$, as shown in (9).

E. Range IFFT

With near perfect phase compensation of all range modulation, the range inverse Fourier transform (IFFT) collapses to the focused range envelope $S_0(\cdot)$ at the correct range position $2r/c$, leaving only azimuth phase terms. Letting the subscript c denote that the output pulse in the associated direction has been compressed, we find

$$p_C P(\tau, f) = \mathbb{C}a\left(-\frac{r\lambda f}{2V^2(r)}\right) S_0\left(\tau - \frac{2r}{c}\right) \cdot \exp\left\{-j\frac{4\pi}{\lambda} r\left[1 - \left(\frac{\lambda f}{2V(r)}\right)^2\right]^{1/2} - j\Theta_\Delta(f; r)\right\} \quad (20)$$

which is to be matched by the third and final phase multiply.

F. Azimuth Filter and Phase Residual

The first phase term of (20) is the normal Doppler modulation. It is this term that must be matched to focus each signal in azimuth. It is a single-valued two-dimensional quantity known over the domain. The final phase term, given by (17), has a known value over the range/Doppler domain [16], [20]. It is a residual generated by the original chirp scaling phase multiply. The required compensation is the conjugate of (20), so that the phase multiplier needed to complete the algorithm is given by

$$\Phi_3(\tau, f) = \exp\left\{-j\frac{2\pi}{\lambda} c\tau\left[1 - \left[1 - \left(\frac{\lambda f}{2V(r = \tau c/2)}\right)^2\right]^{1/2}\right] + j\Theta_\Delta(f; r)\right\} \quad (21)$$

where scatterer range r and the range time coordinate τ are interchangeable since range compression and RCMC have been completed at this stage. Phase compensation may be allowed to vary with range in the range image/Doppler domain, and thus to accommodate satellite or other nonrectangular viewing geometries, as justified in Appendix B. Also, an additional phase compensation could be used at this point to correct for phase error caused by range filter mismatch due to range invariance, for example. (See Appendix C.)

In the range image/Doppler domain, azimuth frequency-dependent bandpass and filter operations may be introduced, such as weighting and look extraction.

G. Azimuth IFFT

The algorithm is completed by an azimuth inverse FFT. Noting that the compressed azimuth impulse response is the suitably scaled and transformed envelope $A(t)$ of the antenna weighting [9], the image impulse response $p_C p_C(\tau, t)$ for zero azimuth offset may be written

$$p_C p_C(\tau, t) = \mathbb{C} S_0(\tau - 2r/c) A(t). \quad (22)$$

H. Comment

In (16), the azimuth reference frequency was chosen to be zero for simplicity. The algorithm is valid when nonzero azimuth reference frequency is used, which is the case for the experiments reported below. As is true for most SAR processors, for squinted data, the Doppler centroid frequency of the azimuth antenna pattern must be used to unwrap the frequencies in the compensations used to rectify signal and image domain. This requires knowledge of the integer and the fractional part of the Doppler ambiguity.

IV. Image Quality: Point Target Simulations

In order to qualify the chirp scaling (CS) algorithm for anticipated requirements of satellite SAR processing, one of the most demanding of the new sensors, RADARSAT [18] was selected for testing. RADARSAT combines high resolution with wide swaths in various modes, and can exhibit large variations in Doppler centroid over the swath. In this section, the results of simulation runs using RADARSAT parameters with the CS and R/D algorithms are presented. The parameters of RADARSAT relevant to the simulation are shown in Table I.

TABLE I
Typical System Parameters Used for Simulation Tests
(Modes Refer to Those of RADARSAT)

Parameter	Fine Resolution Mode	Wide Swath Mode	Units
Radar frequency	5.3	5.3	GHz
Range sampling rate	32.2	12.9	MHz
Chirp FM rate	0.70	0.27	MHz/μsec
Chirp duration	43	43	μsec
Ground range swath width	50	150	Km
Change in azimuth focus parameter $V^2(r)$ from near range to far range	0.24	0.70	%

A. High-Resolution/Wide-Swath Tests

High resolutions provide a demanding test for an algorithm because of increased focusing sensitivities. For this test, RADARSAT's Fine-Resolution mode was used, with resolutions of 7 m. Wide swaths provide a demanding test because range-dependent parameters undergo their largest changes, and processors do not always cope with these range variations accurately. In the context of the CS algorithm, the wide swath introduces the largest nonlinearity in the frequency of the range perturbation function, especially with the lowest incidence angle beams where the rate of change of $V(r)$ is the largest. To test this aspect, RADARSAT's Wide-Swath mode was chosen, with a 150 km ground range swath width.

In each case, single-look complex (SLC) images were studied to yield the most sensitive measurement of image quality parameters. Near and far ranges were simulated to get the maximum range variations. Also, squint angles of 0°, 4°, and 8° were simulated to demonstrate the robustness of the algorithm with respect to squint.

In each mode, the degree of polynomial required to fit the range chirp scaling function was determined experimentally. This was done by finding the error in the fit over the whole swath width using different degrees in the polynomial, and selecting the lowest degree which would introduce negligible effects in subsequent processing of the SAR data. This turned out to be a cubic polynomial in each case.

For each test, an initial point scatterer was placed at the center of the swath to serve as an image quality reference. All range-variant processing parameters were tailored to this reference, as it would be optimally focused. Likewise, for the CS algorithm, the differential RCMC would be zero for this case. Image quality parameters of all other signals were measured against those for the reference. Simulated scatterers were placed at the near and far swath edges, so that the most severe differential range cell migration was simulated. The entire swath was processed in one block, without the use of parameter invariance regions which are a source of error in many algorithms.

The simulated signals were compressed, and their image quality parameters were measured. The key parameters are impulse response width (IRW), geometric registration, phase angle, peak magnitude, maximum sidelobe, and integrated sidelobe ratio (ISLR). No weighting was used in either the range or azimuth directions so that weighting would not be a factor in the algorithm comparisons, and so that the most sensitive measurements could be made.

B. Simulation Results

Experimental results for the Fine-Resolution SLC and Wide-Swath SLC modes and at the minimum and maximum incidence angles are summarized here. At a squint of 8°, and using the Doppler centroid as the reference frequency, the following results were obtained.

1) The range IRW broadening was less than 0.7% compared to the resolution of the reference. Contributing factors to the broadening were measurement error, and the range filter mismatch due to its range-invariance assumption in the implementation. The broadening is less than has been obtained from any other wide-swath, strip-mode SAR processing algorithm, including the R/D algorithm.

2) The azimuth broadening of all responses was less than 0.4% compared to the resolution of the reference target.

3) The range and azimuth registration errors were too small for measurement in all experiments.

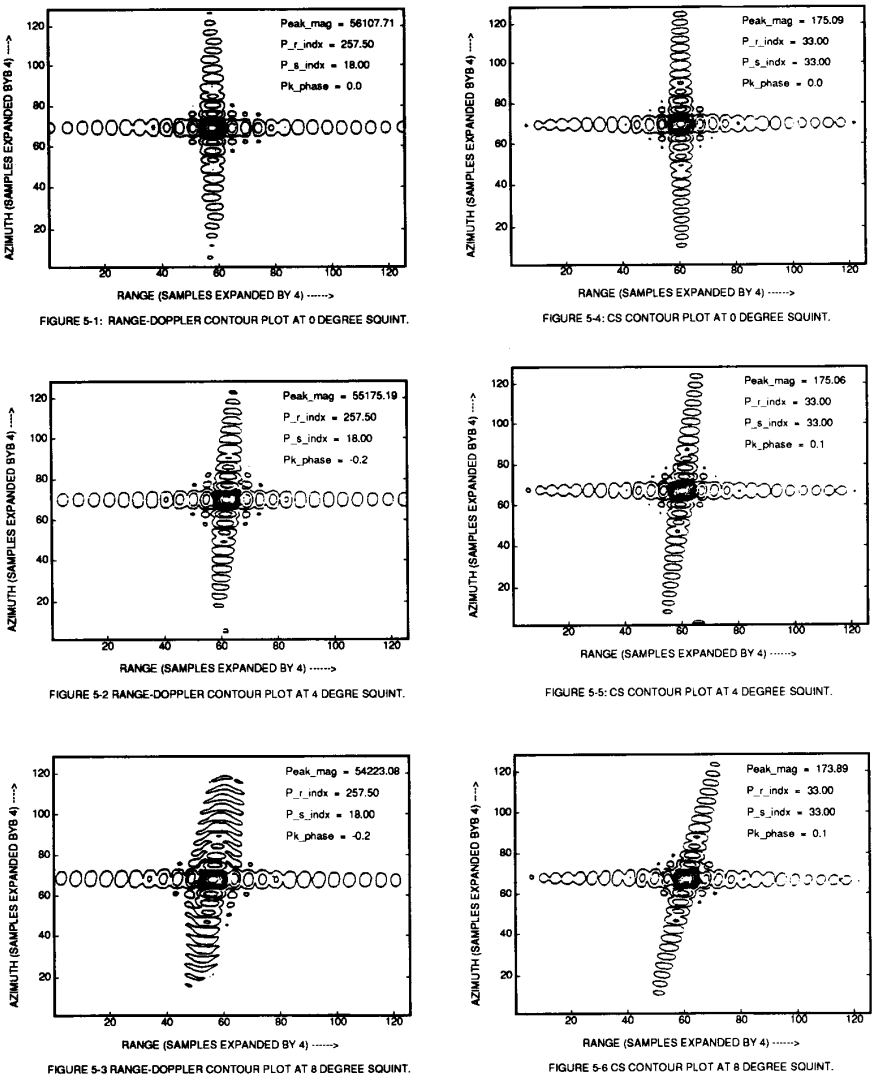

Fig. 5. Contour plots of impulse responses (simulated signals) for the range/Doppler and the chirp scaling algorithms.

4) The phase error for all responses, after correcting for the range filter mismatch, was less than 0.5°.

5) The maximum sidelobe ratio was less than −13 dB, as expected for the Fourier transform of a rectangular window. The one-dimensional ISLR was less than −10 dB.

Fig. 5 is an image domain contour plot of a typical compressed test signal for three angles of squint: 0°, 4°, and 8°. For purposes of comparison, the impulse responses of a precision R/D processor are also shown. The R/D processor used an eight-point RCMC interpolator and included range-time, azimuth-frequency-independent secondary range compression. In addition to improved resolution, the sidelobe structures of the contour plots in Fig. 5 show that the phase matching of the chirp scaling algorithm is superior to that of the R/D algorithm, especially as squint increases.

C. Doppler Centroid Variation Tests

Finally, the effects were studied of choosing the azimuth reference frequency to be different from the Doppler centroid of the simulated signal array. The ideal reference frequency f_{ref} would be equal to the Doppler centroid frequency f_{DC} at each range. However, due to the fact that Doppler centroid frequency can vary with range and that f_{ref} is range invariant in the implementation, in general a difference exists between f_{ref} and f_{DC} as a function of range. The maximum difference is one half the maximum PRF excursion between near and far range, plus 0.2 PRF

allowed for Doppler centroid estimation error. (The maximum excursion is 2.3 PRF's for RADARSAT's Wide-Swath Mode at 4° squint.) The value of f_{ref} usually is chosen to be the midrange f_{DC}, in which case the maximum error between the two frequencies at either edge of the swath is 1.35 PRF's. The squint angle of 4° was chosen to simulate a realistic RADARSAT case.

Experimental results when the reference azimuth frequency f_{ref} differed by as much as 1.4 PRF's from the Doppler centroid f_{DC} show an increase in residual phase error to 4°. All other image quality parameters were comparable to the reference experiments. The phase error was found to be a function of the squint angle, the difference between f_{ref} and f_{DC}, the difference between the scatter range and the reference range, and the rate of change in $V^2(r)$ with range time. A 4° phase error should be acceptable for most applications; this could be compensated easily if required.

V. Image Quality: SAR Examples

To test the image quality properties of the CS algorithm, a scene from Seasat was processed using both the CS algorithm and the precision R/D algorithm. Seasat was selected over ERS-1 because its larger synthetic aperture provides a more demanding test for the algorithms. Each image was produced as an SLC image file. The data were magnitude detected, and then groups of four adjacent azimuth pixels were summed to produce images with a square aspect ratio, a spatial domain process with statistical results similar to those of conventional frequency-selective four-look processing. The image processed with the CS algorithm is shown in Fig. 6. Based on appearance, there is no distinguishing difference noted between it and the corresponding R/D processed scene (not shown). No artifacts were observed in either image; stripes, banding, echoes, and other types of unwanted features are not evident. The radiometry is continuous in both the range and azimuth directions. From this, it is concluded that as far as visual image quality is concerned, the CS algorithm is at least comparable to the reference R/D algorithm.

A radiometric comparison was done using 256 × 256 chips extracted from the two image files. The mean, standard deviation, and their ratio were computed. The results from the two algorithms were within 0.2% of each other. The shapes of the two histograms were essentially identical. Likewise, the range and azimuth spectra of images from the two algorithms were found to be comparable.

From the simulation results of the previous section, the detailed impulse response performance of the CS algorithm should yield better results than those of a precision R/D algorithm. To test this point, the well-known array of Goldstone corner reflectors observed by Seasat were processed by both the CS algorithm and the reference R/D processor. SLC images were produced. The corner reflector responses were analyzed, and the results are summarized in Table II. (Although the absolute radiometric values may be suspect due to possible small-signal suppression, the impulse response widths and relative sidelobe norms have been shown to be useful for the Seasat Goldstone scene [3].)

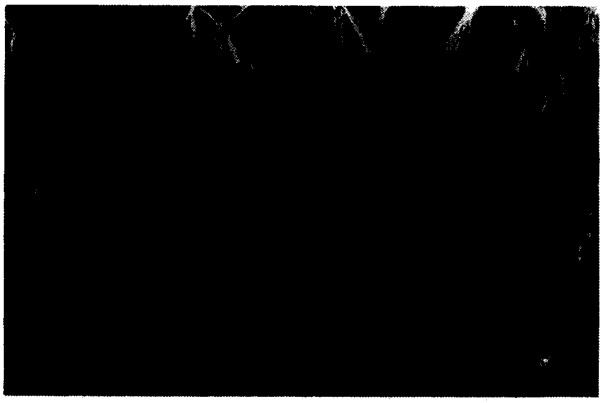

Fig. 6. Seasat scene of Vancouver processed by the chirp scaling algorithm.

Range and azimuth resolutions were each averaged over the six corner reflectors, with better performance of the CS algorithm observed in both dimensions (units in the table are in the original sample spacing of the single look complex image file). The results of this test showed that the range resolution of the CS algorithm is 4.4 percentage points better than the R/D algorithm, and the azimuth resolution is 3.3 percentage points better. This improvement, attributed to the more accurate RCMC and SRC in the CS algorithm, is considered to be significant, as the specification for processor-induced broadening in a SAR application is typically on the order of 7% or less.

The integrated sidelobe ratio (ISLR) in the range and azimuth directions were also averaged over the six corner reflectors, with comparable performance being obtained from the two algorithms. This serves mainly to show that different weightings have not been used to distort the resolution comparisons.

An additional sensitive test of image quality concerns phase consistency. In order to assess the impact of processor-induced phase continuity and relative phase errors, each image was processed twice, with the input data spatially shifted between runs in range and in azimuth. This shift would tend to emphasize any systematic phase errors related to image registration during the compression operation due, for example, to range invariance. The phases of the resulting pairs of image files were compared on a pixel-by-pixel basis. For both the CS algorithm and the precision R/D algorithm, the rms phase difference between pixels was only 3°, indicating that each algorithm has excellent phase consistency.

VI. Implementation Considerations

A. Sensitivity to Errors in Processing Parameters

In SAR processing, a number of parameters have to be well matched in order to achieve accurate focusing. These

TABLE II
COMPARISON BETWEEN CHIRP SCALING (CS) AND RANGE/DOPPLER (R/D) ALGORITHMS. THE R/D ALGORITHM IS A PRECISION VERSION, USING SECONDARY RANGE COMPRESSION, AND THE COMPARISON IS DONE WITH CORNER REFLECTORS IN THE GOLDSTONE SEASAT SCENE.

Target	Algorithm	Range Resolution (cells)	Azimuth Resolution (cells)	Range ISLR (dB)	Azimuth ISLR (dB)
1	CS	1.165	1.251	−10.3	−13.2
	R/D	1.192	1.272	−10.5	−12.9
2	CS	1.242	1.294	−7.3	−10.0
	R/D	1.272	1.299	−7.5	−9.8
3	CS	1.243	1.295	−11.3	−13.7
	R/D	1.292	1.373	−11.2	−13.1
4	CS	1.187	1.376	−8.5	−12.0
	R/D	1.223	1.362	−9.3	−12.5
5	CS	1.232	1.283	−12.9	−12.6
	R/D	1.351	1.438	−11.9	−11.7
6	CS	1.164	1.236	−7.0	−6.2
	R/D	1.227	1.248	−7.7	−6.4
Average	CS	1.206	1.289	−9.6	−11.3
	R/D	1.259	1.332	−9.7	−11.1
Standard Deviation	CS	0.038	0.049	2.3	2.8
	R/D	0.058	0.072	1.8	2.6

include the range and azimuth FM rates and the Doppler centroid. It has been found that the chirp scaling (CS) algorithm shares the same sensitivity to errors in these parameters as the R/D algorithm, with two minor exceptions.

As the CS algorithm relies upon the linearity and knowledge of the slope of the range chirp phase, errors in RCMC could be created by incorrect knowledge of the parameters of the range chirp. However, analysis has shown that the CS algorithm is relatively insensitive to slope errors or nonlinearities in the range chirp. For example, loss of focus in the range compression operation will occur before loss of focus is noted in the RCMC operation, so that if the chirp parameters are known accurately enough for range focusing, then the chirp scaling method of RCMC will be accurate.

Second, the range chirp FM rate affects the residual phase compensation. However, the effect was found to be very small, causing at most a 2° phase error for the maximum range FM rate errors expected in RADARSAT.

B. Computational Efficiency

Since only FFT's and multiplications are used, the implementation in software as well as hardware is relatively straightforward. In the case of a software processor, a few pages of code suffice for the core signal processing operations, while for a hardware processor, only FFT, vector multiplication, and memory units are necessary. Due to the two-dimensional nature of the algorithm, it is easily implemented on a modern workstation with large memory, e.g., 256 Mb or more. It is also well suited to massively parallel main frame machines such as the CM-5 [12] since the FFT's and multiples may be implemented in parallel.

In the absence of significant Doppler variation, the CS algorithm requires about 5% less arithmetic than the R/D algorithm, a saving mainly due to the removal of the eight-point RCMC interpolator. The CS algorithm requires two more corner turns than the R/D algorithm, but that factor is less significant with modern hardware with large solid-state memories.

C. Block Processing

In all SAR processing algorithms, absolute or unaliased azimuth frequency must be used in the parameter calculations. Thus, in SAR processing algorithms that operate in the two-dimensional frequency domain, the variation of Doppler centroid with range imposes an upper limit on the range block size that can be processed. This sometimes necessitates using a smaller block size for such algorithms than would be chosen from efficiency considerations alone.

In the CS algorithm, this implies that smaller range blocks must be used between the range FFT and the range IFFT. The governing block size is determined after the range matched filter throwaway region is discarded, so the range chirp length is not a factor in selecting the block size.

For RADARSAT, up to three range blocks are required to accommodate all imaging modes over all expected squint conditions. Three blocks may be implemented readily in an operational CS processor. The Doppler variation is not a controlling issue for most ERS-1 data when it is operated in yaw-steering mode. For an *L*-band sensor like Seasat, the full-range swath usually can be focused in one block because the relative Doppler centroid variations are fewer than those at *C* band.

When significant Doppler variation must be accom-

modated, the CS algorithm requires a slightly larger memory and processing time than an R/D processor would need under the same conditions. For the range of parameters experienced by the various RADARSAT modes, where the Doppler centroid can vary by up to 2.3 PRF's, the extra memory ranges from about 1 to 10%, and the extra computing can be up to 5% higher than that of the reference R/D processor.

D. Range-Varying Velocity Parameter

From (7), for narrow beam systems, the range cell migration (in meters) is approximately

$$\Delta r = \frac{\lambda^2}{8} \frac{r}{V^2(r)} f^2. \tag{23}$$

Monochromatic wavenumber domain processors neglect both the r and the $V(r)$ dependencies within a block since range parameters must hold the same value for all members in the frequency domain. The chirp scaling algorithm neglects only the range dependence through $V(r)$. It follows that the chirp scaling method is much less sensitive to errors in this parameter.

Consider the following example. For typical geometries at 800 km altitude, the relative sensitivities of the $V(r)$ term and the r terms are

$$\frac{\partial V^2(r)}{\partial r} \frac{1}{V^2(r)} \simeq 6 \cdot 10^{-8}\ \mathrm{m}^{-1} \quad \text{and}$$

$$\frac{\partial r}{\partial r} \frac{1}{r} \simeq 1.2 \cdot 10^{-6}\ \mathrm{m}^{-1}. \tag{24}$$

Hence, setting $V(r) = \text{const}$ and allowing a variable r introduces 20 times less residual range cell migration correction error than does setting both $V(r)$ and r to constant values. When this error is the governing constraint, range block size for the chirp scaling algorithm could be much larger than for the other wave domain techniques.

E. Doppler Estimation

The Doppler estimator can be incorporated into the CS algorithm just as easily as in the R/D case, and the Doppler centroid estimator may be done after the azimuth FFT on range uncompressed data with no adverse effects on accuracy.

F. Weighting

To achieve a shift of the range signal, the chirp scaling phase multiply in (14) introduces a frequency shift in the range spectrum. In order to avoid spectral overlap in the two-dimensional frequency domain, this shift must not exceed half the margin between the range sampling frequency and the range bandwidth. A similar argument shows, due to the small range-variant frequency shift introduced by the chirp scaling multiplier, that the range bandwidth of the signal will be slightly altered. Although this effect is offset later in the processing sequence by the phase multiply of (21), in principle, the frequency weighting of the envelope of the multiplier of (19) should take this into consideration. However, for RADARSAT parameters, the effect is negligible. The fractional change in range bandwidth is equal to the number of range cells in the differential RCMC divided by the range chirp length in cells, which is only 0.003 for RADARSAT. Thus, the potential bandwidth expansion due to the chirp scaling algorithm is about 0.3%.

VII. Conclusions

The chirp scaling (CS) algorithm is a new method of SAR processing in which the range cell migration correction (RCMC) operation is efficiently and accurately implemented by a range-time, azimuth-frequency-domain multiply, thereby eliminating the traditional interpolation operation. The multiply uses the linear FM property of the range chirp to scale (i.e., differentially shift) the radar data in the range direction, achieving the desired range-time and azimuth-frequency-dependent correction.

The CS algorithm has been analyzed theoretically and experimentally, and has been found to be an appealing approach to precision SAR processing, particularly when high accuracy is needed in the single-look complex image product. In the experiments, the accuracy and image quality of the CS algorithm compare favorably with the precision R/D algorithm. An improvement in range resolution was measured, mainly due to the more accurate method of RCMC and SRC employed. The CS algorithm is capable of high performance over a relatively wide range of parameters, even for squinted data, and at a small increment in cost when compared to current methods.

Appendix A
Chirp Scaling Principle

The scaling principle applies to a large time–bandwidth, linearly frequency-modulated signal [13], and is briefly summarized here. Consider a one-dimensional signal with linear FM modulation (chirp) of rate K_s and phase center at $\tau = \tau_1$ as

$$\exp\{-j\pi K_s(\tau - \tau_1)^2\}. \tag{A-1}$$

The phase structure of this signal may be slightly reshaped by multiplying with another linearly modulated signal having an FM rate C_s that is a small fraction of that of the original signal. The multiplicand is

$$\Phi_1 = \exp\{-j\pi C_s K_s \tau^2\}. \tag{A-2}$$

The result, after multiplication of the two modulated signals, is

$$\exp\{-j\pi K_s[(1 + C_s)\tau^2 - 2\tau_1\tau + \tau_1^2)]\} \tag{A-3}$$

which is a chirp signal resembling the original, but with a new phase center

$$\tau_1' = \frac{1}{1 + C_s} \tau_1 \tag{A-4}$$

and new chirp rate

$$K_s' = K_s(1 + C_s). \tag{A-5}$$

The position of the new phase center is proportional to τ_1, and thus is scaled linearly. The new chirp rate is known, and in the chirp scaling algorithm, is matched, to lead to range signal focus, during range compression. A consequence of the chirp scaling multiply is that the phase of the signal at the new phase center is

$$-\pi K_s \frac{C_s}{1 + C_s} \tau_1^2 \tag{A-6}$$

which, having a known value, may be eliminated by a final phase multiply.

Appendix B
Use of a Nonlinear Range Perturbation Function

The chirp scaling multiplier or range perturbation function (RPF) of (14) is exactly linear FM (i.e., quadratic function of τ) only if the following two conditions are satisfied:

1) the radar pulse is linear FM, and
2) the azimuth FM rate parameter $V(r)$ is range invariant.

In practice, $V(r)$ varies with range, and the range chirp may have a nonlinear component. To handle this case accurately, a nonlinear component can be added to the frequency of the RPF by expressing the phase of the RPF as a polynomial in range time:

$$\Phi_1(\tau, f, r_{\text{ref}}) = \exp\{-j(a_0 + a_1\tau_1 + a_2\tau_1^2 + a_3\tau_1^3 + \cdots\} \tag{B-1}$$

where $\tau_1 = \tau - \tau_{\text{ref}}$. The coefficients a_i are a function of azimuth frequency f and the reference range r_{ref}, and for the linear RPF case, all coefficients are zero except a_2, which is equal to $\pi K_s C_s$ as in (14) of the text.

In the RADARSAT experiments, the RPF frequency was approximated by a cubic polynomial (i.e., the RPF phase was a quartic function of τ_1 [25]).

The *spectrum* of the perturbed signal can be obtained analytically by an approximation that the frequency of the RPF is locally linear, i.e., the RPF is approximated by

$$\Phi_1'(\tau, f, r_{\text{ref}}) \approx \exp\{-j(g_0\tau_1 + g_1\tau_1^2)\}. \tag{B-2}$$

The coefficients g_0 and g_1 are functions of range; they depend upon the local slope of the RPF frequency. Note that g_0 is zero and g_1 is range independent ($= \pi K_s C_s$) if the frequency of the RPF is perfectly linear, as in (14). Note also that (B-2) is equivalent to changing the reference range for each value of τ.

Letting

$$D(f, r) = \sqrt{1 - \left(\frac{\lambda f}{2V(r)}\right)^2}, \tag{B-3}$$

the two-dimensional spectrum of the perturbed signal is given by

$$\begin{aligned} PP(f_\tau, f) = {} & \mathbb{C}a\left(-\frac{r\lambda f}{2V^2}\right) s_0\left(-\frac{f_\tau}{K_s(1 + C_s)}\right) \\ & \cdot \exp\left[-j\frac{4\pi}{\lambda} rD(f, r)\right] \\ & \cdot \exp\left[+j\pi \frac{D(f, r) f_\tau^2}{K_s(f; r_{\text{ref}})}\right] \exp\left[-j\frac{4\pi}{c} f_\tau r\right] \\ & \cdot \exp\left[-j\frac{4\pi}{c}\left(\frac{1}{D(f, r_{\text{ref}})} - 1\right) r_{\text{ref}} f_\tau\right] \\ & \cdot \exp\left[-j\frac{4\pi K_s(f; r_{\text{ref}})}{c^2} \frac{g_1}{\pi K_s(f; r_{\text{ref}}) + g_1} \right. \\ & \left. \cdot \left(\frac{r}{D(f, r)} - \frac{r_{\text{ref}}}{D(f, r_{\text{ref}})} + \frac{cg_0}{4g_1}\right)^2 - j\frac{g_0^2}{4g_1}\right]. \end{aligned} \tag{B-4}$$

Compared to the linear frequency RPF case, the residual phase represented by the last exponential term in (B-4) is slightly modified to account for the local linearization process.

Appendix C
Phase Error of Compressed Signal due to Range Matched Filter Invariance

Although all intrinsic errors in the CS algorithm are small, the largest error in the algorithm is the range-invariant assumption of the range matched filter. Theoretically, the range matched filter varies with range due to range-variant matched filter FM rate K_s. In this Appendix, we derive a phase correction factor to remove the main manifestation of this range-invariance assumption. (Note that the range/Doppler algorithm also experiences this error, and could be corrected in the same way.)

Let ΔK_s be the error in the FM rate due to the range-invariant assumption of K_s. It introduces two errors: range broadening and phase errors, with the latter being the more prominent of the two. The phase error $\Delta\phi$ at the edge of the matched filter function is given by

$$\Delta\phi = \pi \Delta K_s \left(\frac{T}{2}\right)^2 \tag{C-1}$$

where T is the pulse duration. The *phase error* $\Delta\gamma$ after compression can be obtained by noting that the value of the compressed pulse at its peak is given by

$$x(0) = \int_{-T/2}^{+T/2} e^{-j\pi\Delta K_s u^2}\, du. \tag{C-2}$$

By expanding the phase of $x(0)$ in a power series [2], [11] the phase error $\Delta\gamma$ is found to be

$$\Delta\gamma = -\frac{\Delta\phi}{3} + 0.0028\Delta\phi^3 + \cdots \approx -\frac{\Delta\phi}{3}. \tag{C-3}$$

[The same result has been obtained by Wong (unpublished).] The value of $\Delta\gamma$ can be computed as a function of range, and thus the phase error can be corrected in the compressed image.

For RADARSAT, the typical phase error of the edge of the matched filter function is less than 10° for the Fine-Resolution beams. This gives less than 1% broadening in the compression process. The phase error after compression is about 3°, which can be corrected using (C-3).

REFERENCES

[1] R. Bamler, "A comparison of range-Doppler and wave-number domain SAR focusing algorithms," *IEEE Trans. Geosci. Remote Sensing*, vol. 30, pp. 706–713, July 1992.

[2] R. Bamler and D. Just, "Phase statistics and decorrelation in SAR interferograms," in *Proc. IEEE Geosci. Remote Sensing Symp., IGARSS'93*, Tokyo, Japan, Aug. 1993, pp. 980–984.

[3] A. D. Goldfinger, "Seasat SAR processor signatures: Point targets," Rep. JHU/APL CP 078, Appl. Phys. Lab., The Johns Hopkins Univ., Laurel, MD, Apr. 1980.

[4] M. Born and E. Wolf, *Principles of Optics*. New York: Pergamon, 1959, Appendix III.

[5] C. Cafforio, C. Prati, and F. Rocca, "SAR focusing using seismic migration techniques," *IEEE Trans. Aerosp. Electron. Syst.*, vol. 27, no. 2, pp. 194–207, 1991.

[6] ——, "Full resolution focusing of Seasat SAR images in the frequency-wavenumber domain," *Int. J. Remote Sensing*, vol. 12, pp. 491–510, 1991.

[7] C. Y. Chang, M. Jin, and J. C. Curlander, "Squint mode SAR processing algorithms," in *Proc. IEEE Geosci. Remote Sensing Symp., IGARSS'89*, Vancouver, Canada, 1989, pp. 2584–2587.

[8] I. Cumming, F. Wong, and R. K. Raney, "A SAR processing algorithm with no interpolation," in *Proc. IEEE Geosci. Remote Sensing Symp., IGARSS'92*, Clear Lake, TX, May 1992, pp. 376–379.

[9] R. O. Harger, *Synthetic Aperture Radar: Theory and Design*. New York: Academic, 1970.

[10] M. Y. Jin and C. Wu, "A SAR correlation algorithm which accommodates large range migration," *IEEE Trans. Geosci. Remote Sensing*, vol. GE-22, pp. 592–597, Nov. 1984.

[11] D. Just and R. Bamler, "Phase statistics in interferograms," submitted to *Appl. Opt.*, 1993.

[12] Y. Luo, I. G. Cumming, and M. Yedlin, "Benchmarking a massively parallel computer by a synthetic aperture radar processing algorithm," in *Proc. 3rd Int. Conf. Appl. Supercomput. in Eng., ASE'93*, Bath, England, Sept. 1993.

[13] A. Papoulis, *Systems and Transforms with Applications in Optics*. New York: McGraw-Hill, 1968, pp. 203–204.

[14] R. K. Raney, "Considerations for SAR image quantification unique to orbital systems," *IEEE Trans. Geosci. Remote Sensing*, vol. 29, no. 5, pp. 754–760, 1991.

[15] ——, "A new and fundamental Fourier transform pair," in *Proc. IEEE Geosci. Remote Sensing Symp., IGARSS'92*, Clear Lake, TX, May 1992, pp. 106–107.

[16] ——, "An exact wide field digital imaging algorithm," *Int. Remote Sensing*, vol. 13, no. 5, pp. 991–998, 1992.

[17] R. K. Raney and P. W. Vachon, "A phase preserving SAR processor," in *Proc. IEEE Geosci. Remote Sensing Symp., IGARSS'89*, Vancouver, Canada, July 1989, pp. 2588–2591.

[18] R. K. Raney, A. P. Luscombe, E. J. Langham, and S. Ahmed, "RADARSAT," *Proc. IEEE*, vol. 79, pp. 839–849, June 1991.

[19] H. Runge and R. Bamler, "A novel method for range migration correction for SAR," in *Proc. IEEE Geosci. Remote Sensing Symp., IGARSS'91*, Espoo, Finland, July 1991, p. 1435.

[20] ——, "A novel high precision SAR focusing algorithm based on chirp scaling," in *Proc. IEEE Geosci. Remote Sensing Symp., IGARSS'92*, Clear Lake, TX, May 1992, pp. 372–375.

[21] A. M. Smith, "A new approach to range-Doppler SAR processing," *Int. J. Remote Sensing*, vol. 12, pp. 235–251, 1990.

[22] R. Stolt, "Migration by Fourier transform techniques," *Geophys.*, vol. 43, no. 1, pp. 49–76, 1978.

[23] M. R. Vant, G. E. Haslam, and G. M. Royer, "A digital signal processing approach for satellite-borne synthetic aperture radar (SAR)," in *Proc. Int. Conf. Radar*, Paris, France, Dec. 1978, pp. 251–256.

[24] F. H. Wong and I. G. Cumming, "Error sensitivities of a secondary range compression algorithm," in *Proc. Geosci. Remote Sensing Symp., IGARSS'89*, Vancouver, Canada, July 1989, pp. 2584–2587.

[25] F. H. Wong, I. G. Cumming, and R. K. Raney, "Processing simulated RADARSAT SAR data with squint by a high precision algorithm," in *Proc. IEEE Geosci. Remote Sensing Symp., IGARSS'93*, Tokyo, Japan, Aug. 1993, pp. 1176–1178.

[26] C. Wu, "A digital system to produce imagery from SAR data," in *Proc. AIAA Syst. Design Driven by Sensors Conf.*, Oct. 1976.

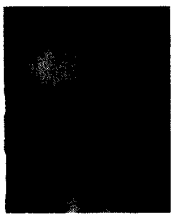

R. Keith Raney (F'91) received the B.S. degree (cum laude) from Harvard University, in 1960, the M.S. degree in electrical engineering from Purdue University, in 1962, and the Ph.D. degree in computer, information, and control from the University of Michigan in 1968. His dissertation was in the area of nonlinear systems theory applied to radar modeling.

He was with the Canada Centre for Remote Sensing (CCRS) from 1976 to 1994. He was a cofounder of RADARSAT, Canada's first remote sensing satellite program, and was its Chief Radar Scientist from 1981 to 1989. He contributed to the algorithm design for the first digital processor for Seasat SAR data, and participated in the conceptual design phase of radar systems for Apollo 16, Pioneer Venus, Magellan, RADARSAT, ERS-1, and SIR-C, as well as several airborne radar programs. He was Principal Investigator for the LIMEX'89 project, an international remote sensing experiment in the marginal ice zone of Canada's Atlantic Coast. He founded the CCRS Tropical Forest Initiative, a major element of which was SAREX, a multinational radar experiment in Latin and South America. He is the author or coauthor of more than 200 papers in the field of imaging radar and applications, including the article on radar in *The Canadian Encyclopedia*. Dr. Raney joined the Space Department of the Applied Physics Laboratory, The Johns Hopkins University, in July 1994.

Dr. Raney is a Past President of the IEEE Geoscience and Remote Sensing Society, and a Fellow of the Electromagnetics Academy.

H. Runge, photograph and biography not available at the time of publication.

Richard Bamler received the Diploma degree in electrical engineering, the Eng.Dr. degree, and the "habilitation" in the field of signal and systems theory in 1980, 1986, and 1988, respectively, all from the Technical University of Munich, Germany.

He worked at that University during 1981 and 1988 on optical signal processing, holography, wave propagation, and tomography. He is the author of a textbook on multidimensional linear systems. He joined the German Remote Sensing Data Center (DFD) at the German Aerospace Research Establishment (DLR), Oberpfaffenhofen, in 1989, where he is currently a Group Supervisor for SAR algorithm development. He has designed the processing algorithms for the German X-SAR processor. Recently, he was a Visiting Scientist at the Jet Propulsion Laboratory (JPL), where he worked on the processing of data from the SIR-C ScanSAR, along-track interferometry, and azimuth tracking modes.

Ian G. Cumming received the B.Sc. degree in engineering physics from the University of Toronto in 1961, and the Ph.D. degree in computing and automation from Imperial College, University of London, in 1968.

Following work in steel mill automation and sonar signal processing, he joined MacDonald Dettwiler and Associates in 1977. Since that time, he has developed synthetic aperture radar signal processing algorithms, and has worked on systems for processing polarimetric and interferometric radar data, and for the compression of radar data. In 1993 he joined the Department of Electrical Engineering, University of British Columbia, where he holds the MacDonald Dettwiler/NSERC Industrial Research Chair in Radar Remote Sensing. The laboratory supports a research staff of ten engineers and students, working in the fields of squinted SAR processing, satellite two-pass interferometry, airborne polarimetric radar calibration requirements, SAR autofocusing, and Doppler estimation.

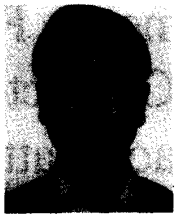

Frank H. Wong received the B.Eng. and M.Sc. degrees in electrical engineering from McGill University in 1969 and Queen's University in 1971, respectively and the Ph.D. degree in computer science from the University of British Columbia in 1984.

He worked in the area of signal processing at the Computing Devices Company prior to joining MDA in 1977. A member of the radar team at MDA, he was extensively involved in the design and study of SAR processing algorithms for both airborne and satellite-borne SAR data, and thus has accumulated over ten years' experience in the field. He currently is studying SAR processing algorithms for RADARSAT.